



Unified description of three-dimensional optical diffraction microscopy: from transmission microscopy to optical coherence tomography: tutorial

ANNE SENTENAC^{1,*} AND JEROME MERTZ² 

¹Aix Marseille Université, CNRS, Centrale Marseille, Institut Fresnel, UMR 7249, 13013 Marseille, France

²Department of Biomedical Engineering, Boston University, Boston, Massachusetts 02215, USA

*Corresponding author: anne.sentenac@fresnel.fr

Received 13 November 2017; revised 14 February 2018; accepted 9 March 2018; posted 13 March 2018 (Doc. ID 313379); published 11 April 2018

In this tutorial, we present a general model linking the data provided by any optical diffraction microscope to the sample permittivity. Our analysis is applicable to essentially all microscope configurations, in transmission or reflection mode, using scanning or full-field illumination, with or without interferometric measurements. We include also a generalization of our analysis to vector fields. © 2018 Optical Society of America

OCIS codes: (180.6900) Three-dimensional microscopy; (110.0110) Imaging systems.

<https://doi.org/10.1364/JOSAA.35.000748>

1. INTRODUCTION

Optical diffraction microscopy is a valuable tool for imaging micrometer-scale objects non-invasively. Since its invention three centuries ago, many configurations have been proposed using a variety of light sources (from white-light lamps to pulsed lasers) and a variety of detection methods (from single detectors to cameras). Basically, two principal modalities have emerged: the scanning mode, which raster scans a focused spot and detects the scattered light with a single detector, and the full-field mode, which illuminates the sample across a full field of view with either coherent or partially coherent light, and detects the scattered light with a camera. As will be discussed below, these configurations are formally equivalent.

The purpose of this paper is to present a general, unified description of optical diffraction microscopy using a common theoretical framework. Our goal is not to delve into the details of the many different microscopy variations, nor to discuss how they can be implemented in practice, but rather to show how seemingly disparate variations can be summarized and categorized using two very basic concepts: the Helmholtz principle of reciprocity and the Green time-reversal identity. Our formalism applies to essentially all diffraction microscopes, whether they be transmitting or reflecting, scanning or full-field, coherent or partially coherent, provided only that they be *linear*. For simplicity, a scalar treatment of light fields is utilized throughout the body of this paper. A fully vectorial treatment is relegated to the appendix.

Most of the results in this paper are not new and have been presented in some form or other in the literature, the most influential of which is the seminal work by Streibl [1]. On the other hand, our translation from a scalar to a fully vector formalism has not, to our knowledge, been presented before in such a condensed form. We begin with a brief overview of the basic principles underlying our discussion, followed by a derivation of the general Green's functions associated with various microscope modalities, followed finally by specific examples making use of lenses and pupils.

2. EQUIVALENCE PRINCIPLES

The following equivalence principles are useful for grouping microscopy techniques together and establishing their commonalities.

A. Equivalence of Continuous and Pulsed Illumination with Equal Spectrum

Assuming that the integration time of the detector is longer than the laser pulse duration, we can invoke Parseval's theorem. The integration over time of a pulse intensity is thus equal to the integration over frequency of the pulse intensity spectrum. We conclude that, regardless of whether the illumination is pulsed or continuous, the imaging properties of a microscope can be analyzed using monochromatic illumination and performing an integration over frequency at the very end of the derivation.

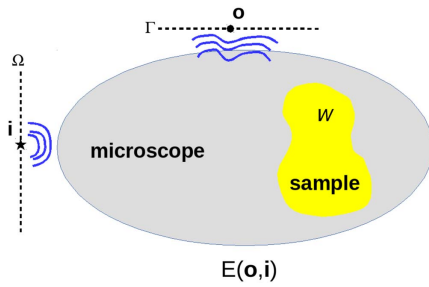


Fig. 1. General configuration of a microscope. The microscope optical elements are depicted in gray while the sample is in yellow. W is the domain over which the permittivity variations resulting from the sample, $\delta\epsilon$, are non-zero. \mathbf{i} is a point source in the illumination domain Ω and \mathbf{o} a detection point of the observation domain Γ .

B. Equivalence of Full-Field Incoherent and Scanning Modes

In a scanning microscope the illumination originates from a single point source, placed at \mathbf{i} , and the field intensity is detected by a single detector, which can be point-like (in the confocal mode) or extended. We call Γ the detector domain over which the field intensity is integrated. In a full-field incoherent microscope the field intensity is detected on camera pixels placed at the observation points \mathbf{o} and the extended illumination is generated by many mutually incoherent point sources. We call Ω the domain of incoherent sources from which the illumination is generated.

Assuming the field to be scalar and satisfying the inhomogeneous Helmholtz wave equation, the reciprocity theorem (derived in Appendix A) states that the field observed at \mathbf{o} radiated by a source placed at \mathbf{i} , $E(\mathbf{o}, \mathbf{i})$ is equal to the field observed at \mathbf{i} radiated by the same source placed at \mathbf{o} , namely, $E(\mathbf{o}, \mathbf{i}) = E(\mathbf{i}, \mathbf{o})$. In the scanning mode, one records $\int_{\Gamma} |E(\mathbf{o}, \mathbf{i})|^2 d^2\mathbf{o}$, while in the full-field mode one records $\int_{\Omega} |E(\mathbf{o}, \mathbf{i})|^2 d^2\mathbf{i}$. If Γ and Ω are made equal, these two measures are identical [2]—see Fig. 1 for an illustration of the microscope.

In the vectorial case, the equivalence between scanning and full-field incoherent modes requires more caution as the polarization of the source must be accounted for (see Appendix B). In practice, scanning and full-field modes are equivalent when polarizers are placed in the illumination and detection paths, or when the three canonical polarizations are used in the scanning mode to account for the unpolarized detection of the full-field mode. To simplify our derivation, we consider only scalar fields in the main body of the paper, and defer an extension of this derivation to vectorial fields in Appendix B.

We conclude that the properties of any diffraction microscope can be obtained by studying only the scanning mode.

3. LINK BETWEEN THE MICROSCOPE MEASUREMENT AND THE SAMPLE

Hereafter, we only consider microscopes in which the illumination is provided by a scalar monochromatic point source of wavelength λ placed at \mathbf{i} and the image data is recorded on a single detector (point-like or extended). To simplify our analysis, we assume that a volumetric image is formed by displacing the sample in three dimensions. In practice, this scanning

technique is seldom utilized, and 3D imaging is generally obtained by movement of the microscope elements, such as tilting mirrors or a translating lens to displace the scanning point. In the ideal case where the optical properties of the microscope are translationally invariant, both approaches are equivalent.

A. Modeling the Field Intensity at the Detector

We define $E(\mathbf{o}, \mathbf{i})$ to be the field observed at the detector position \mathbf{o} in the presence of the sample and $G(\mathbf{o}, \mathbf{i})$ the field observed at \mathbf{o} in the absence of the sample; see Fig. 1. From the different inhomogeneous Helmholtz equations satisfied by E and G (see Appendix A for the derivation), one obtains the exact integral equation for E :

$$E(\mathbf{o}, \mathbf{i}) = G(\mathbf{o}, \mathbf{i}) + k_0^2 \int_W G(\mathbf{o}, \mathbf{r}) \delta\epsilon(\mathbf{r}) E(\mathbf{r}, \mathbf{i}) d^3\mathbf{r}, \quad (1)$$

where $G(\mathbf{o}, \mathbf{r})$ is the field radiated at \mathbf{o} by a point source placed at \mathbf{r} in the absence of the sample, $E(\mathbf{r}, \mathbf{i})$ is the field radiated at \mathbf{r} by the point source at \mathbf{i} in the presence of the sample, $\delta\epsilon$ is the permittivity variation resulting from the sample, and $k_0 = 2\pi/\lambda$. Note that $\delta\epsilon$ is null outside the support of the sample, denoted by W .

According to Eq. (1), the observed field E is non-linearly linked to the sample $\delta\epsilon$, which is a problem endemic to any imaging technique. Fortunately, when the sample is weakly scattering (which is generally the case, for example, with biological samples) one can assume that the field in the sample $E(\mathbf{r}, \mathbf{i})$ is only slightly perturbed relative to the field that would exist in the absence of the sample, $G(\mathbf{r}, \mathbf{i})$. In this case, a linear dependence between the field and sample can be restored with the well-known Born approximation [1,3]:

$$E(\mathbf{o}, \mathbf{i}) = G(\mathbf{o}, \mathbf{i}) + \delta E(\mathbf{o}, \mathbf{i}),$$

$$\delta E(\mathbf{o}, \mathbf{i}) \approx k_0^2 \int_W G(\mathbf{o}, \mathbf{r}) \delta\epsilon(\mathbf{r}) G(\mathbf{r}, \mathbf{i}) d^3\mathbf{r}. \quad (2)$$

But detectors are sensitive to intensities rather than complex fields. The detected intensity is given here by

$$|E(\mathbf{o}, \mathbf{i})|^2 = |G(\mathbf{o}, \mathbf{i})|^2 + |\delta E(\mathbf{o}, \mathbf{i})|^2 + 2\Re[G^*(\mathbf{o}, \mathbf{i}) \delta E(\mathbf{o}, \mathbf{i})]. \quad (3)$$

Thus, the quasi-linearity between the recorded microscope data and the sample resides only within the interference term $2\Re[G^*(\mathbf{o}, \mathbf{i}) \delta E(\mathbf{o}, \mathbf{i})]$. Essentially all microscopes rely on this term to form meaningful images, though with some notable exceptions such as reflectance confocal and dark-field microscopes, whose particularities will be addressed at the end of the discussion.

In general, the performance of a microscope critically depends on its ability to distinguish the interference term from the background. In this regard, interferometric microscopes, which use two independent arms to produce the sample field δE and reference field $G(\mathbf{o}, \mathbf{i})$, represent a better option than non-interferometric microscopes since they provide flexibility in both the phase and amplitude of $G(\mathbf{o}, \mathbf{i})$. By adjusting the phase of $G(\mathbf{o}, \mathbf{i})$, a fully complex measurement of δE can be constructed from a sequence of intensity measurements, thus circumventing the restriction that comes from taking only the real part of the interference term. Moreover, by adjusting

the amplitude of $G(\mathbf{o}, \mathbf{i})$, the reference field can be tuned large enough that the non-linear term $|\delta E(\mathbf{o}, \mathbf{i})|^2$ in Eq. (3) can rigorously be neglected. Optical coherence tomography (OCT) is the most widespread example of this kind of interferometric microscope.

B. Point Spread Functions of Interferometric Microscopes

We assume here that the complex interference term can be extracted from the intensity measurements and provide its connection with the sample permittivity distribution $\delta\epsilon$.

From Eq. (3), we infer that an interferometric microscope with an extended detector Γ and an illumination point source placed at \mathbf{i} provide the complex data:

$$D = \int_{\Gamma} G^*(\mathbf{o}, \mathbf{i}) \delta E(\mathbf{o}, \mathbf{i}) d^2\mathbf{o}, \quad (4)$$

where dependencies on \mathbf{i} are hereafter suppressed.

Translating the sample by $-\mathbf{x}$ in three dimensions yields a 3D image $D(\mathbf{x})$ which, using the expression of δE given by Eq. (2), can be recast as the correlation of $\delta\epsilon$ with a complex point spread function H [4]:

$$D(\mathbf{x}) = \int H(\mathbf{r}) \delta\epsilon(\mathbf{x} + \mathbf{r}) d^3\mathbf{r},$$

$$H(\mathbf{r}) = k_0^2 G(\mathbf{r}, \mathbf{i}) \int_{\Gamma} G^*(\mathbf{o}, \mathbf{i}) G(\mathbf{o}, \mathbf{r}) d^2\mathbf{o}. \quad (5)$$

Equation (5) represents the complex point spread function H of any interferometric microscope. For non-interferometric microscopes, the link between the sample and the recorded data is provided by the real part of D .

When the detector is point-like, the expression for H reduces to

$$H_{\text{point}}(\mathbf{r}) \propto k_0^2 G(\mathbf{r}, \mathbf{i}) G(\mathbf{o}, \mathbf{r}). \quad (6)$$

In a confocal configuration in which \mathbf{i} is conjugated to \mathbf{o} one can further simplify the expression using the reciprocity theorem:

$$H_{\text{confocal}}(\mathbf{r}) \propto k_0^2 G^2(\mathbf{r}, \mathbf{i}). \quad (7)$$

When the detector is so large that it can collect all the light from the microscope, on either the reflected or transmitted side, it is also possible to derive a simplified expression for H .

For this derivation we first define the transmission and reflection sides by introducing a plane that separates the illumination point \mathbf{i} from the sample domain \mathcal{W} . The optical axis z is then defined as the normal to this plane directed from the source to the sample. The extended detector that collects all the light on the reflection (transmission) side, $\Gamma_{R(T)}$, can be modeled as a half-sphere in the far field of the microscope with negative (positive) z , as illustrated in Fig. 2.

Second, we invoke the time-reversal Green identity [5] (see Appendix A), which states that, if the microscope itself (i.e., without the sample) does not cause absorption,

$$\int_{\Gamma_R + \Gamma_T} G^*(\mathbf{o}, \mathbf{i}) G(\mathbf{o}, \mathbf{r}) d^2\mathbf{o} = \frac{1}{2ik_0} [G(\mathbf{r}, \mathbf{i}) - G^*(\mathbf{r}, \mathbf{i})], \quad (8)$$

where $\Gamma_R + \Gamma_T$ is the far-field sphere formed by the union of Γ_R and Γ_T enclosing the microscope.

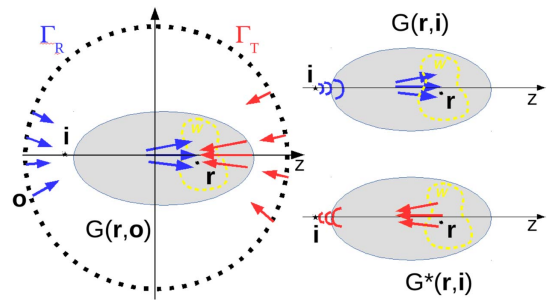


Fig. 2. Illustration of the key assumptions used for deriving the point spread function of a microscope with extended detectors on the transmission, Γ_T , or reflection, Γ_R , side: (1) The microscope without the sample has no absorbing components; (2) (left) the field *in the absence of the sample* created by a point source located on the reflection (transmission) detector at any point inside the sample domain, $G(\mathbf{r}, \mathbf{o})$, is assumed to be a sum of plane waves propagating exclusively in the positive (negative) z directions; (3) (right) the field $G(\mathbf{r}, \mathbf{i})$ created by the illumination source \mathbf{i} at any point inside the sample domain is assumed to be a sum of plane waves propagating exclusively in the positive z direction. As a consequence, $G^*(\mathbf{r}, \mathbf{i})$ is a sum of plane waves propagating toward negative z .

Third, we distinguish the integrals over the half-spheres Γ_R and Γ_T . Because $G(\mathbf{o}, \mathbf{r}) = G(\mathbf{r}, \mathbf{o})$, by virtue of reciprocity, one can interpret the term $\int_{\Gamma_{R(T)}} G^*(\mathbf{o}, \mathbf{i}) G(\mathbf{o}, \mathbf{r}) d^2\mathbf{o}$ as the field observed at \mathbf{r} in the sample domain radiated by sources with amplitude $G^*(\mathbf{o}, \mathbf{i})$ located on the reflection (transmission) detector. In general, this field can be modeled as a sum of plane waves propagating exclusively toward positive (negative) z , as shown in Fig. 2, left. We assume further that $G(\mathbf{r}, \mathbf{i})$ ($G^*(\mathbf{r}, \mathbf{i})$) can also be described as a sum of plane waves propagating exclusively toward positive (negative) z , as shown in Fig. 2, right.

An identification of the waves propagating in the positive (negative) z directions in both sides of Eq. (8) leads to

$$\int_{\Gamma_R} G^*(\mathbf{o}, \mathbf{i}) G(\mathbf{o}, \mathbf{r}) d^2\mathbf{o} = \frac{1}{2ik_0} G(\mathbf{r}, \mathbf{i}),$$

$$\int_{\Gamma_T} G^*(\mathbf{o}, \mathbf{i}) G(\mathbf{o}, \mathbf{r}) d^2\mathbf{o} = -\frac{1}{2ik_0} G^*(\mathbf{r}, \mathbf{i}). \quad (9)$$

Note that Eq. (9) does not require $\Gamma_{R(T)}$ to be half-spheres. A sufficient condition is that the detectors should encompass all the points for which the reference field $G^*(\mathbf{o}, \mathbf{i}) \neq 0$. In other words, the detectors should be large enough to collect all the light propagating toward positive or negative z , *in the absence of the sample*.

Inserting Eq. (9) into Eq. (8) yields the point spread function in the reflection configuration,

$$H_R(\mathbf{r}) = \frac{k_0}{2i} G^2(\mathbf{r}, \mathbf{i}), \quad (10)$$

and in the transmission configuration,

$$H_T(\mathbf{r}) = -\frac{k_0}{2i} |G|^2(\mathbf{r}, \mathbf{i}). \quad (11)$$

The expressions (5)–(7), (10), and (11) are the main results of this paper. They describe the behavior of most existing microscopes as will be discussed in the next section.

4. DISCUSSION

To evaluate the point spread function of a specific microscope, one needs the expression for the field observed at \mathbf{u} created by a point source at \mathbf{v} in the absence of the sample, $G(\mathbf{u}, \mathbf{v})$. In an often encountered situation, \mathbf{u} and \mathbf{v} are situated on opposite sides of a tube lens and objective with pupil function $p_{v \rightarrow u}$ in a $4f$ configuration—see Fig. 3. In this case, a precise expression of G can be obtained using the Weyl expansion of the Green function in a homogeneous medium [6]. Assuming unit magnification, one obtains

$$G(\mathbf{u}, \mathbf{v}) = \frac{i}{8\pi^2} \int \frac{p_{v \rightarrow u}(\mathbf{k}_\perp)}{\gamma} \exp[i\mathbf{k} \cdot (\mathbf{u} - \mathbf{v}')] d^2k_\perp, \quad (12)$$

where $\mathbf{k} = \mathbf{k}_\perp + \gamma \hat{\mathbf{z}}_{v \rightarrow u}$, with $\gamma = \sqrt{k_0^2 - k_\perp^2}$, \mathbf{v}' is the conjugate point of \mathbf{v} , and $\hat{\mathbf{z}}_{v \rightarrow u}$ is the unit vector along the optical axis oriented from \mathbf{v} to \mathbf{u} . We note that G , which is the field created by a point source (i.e., a Green function), differs from the generally used amplitude point spread function, which is a field propagation operator, essentially by a factor of i . The pupil function $p_{v \rightarrow u}$ has a bounded support in the transverse Fourier plane normal to $\hat{\mathbf{z}}_{v \rightarrow u}$ (encompassed by \mathbf{k}_\perp). It is usually a disk of radius $k_0 \text{NA}$, where $\text{NA} = \sin \theta$ is the numerical aperture of the objective with collection angle θ . In this case, the support of the 3D Fourier transform of $G(\mathbf{u}, \mathbf{v})$ with respect to \mathbf{u} is a cap of sphere of radius k_0 in the positive $\hat{\mathbf{z}}_{v \rightarrow u}$ half-space, whose projection onto the plane normal to $\hat{\mathbf{z}}$ is a disk of radius $k_0 \text{NA}$, as illustrated in Fig. 3.

Inserting Eq. (12) into Eqs. (5)–(7), (10), and (11) permits the calculation of the point spread function H of most scanning or full-field microscopes. Hereafter, we provide a simple analysis of the resolution of several microscopes by estimating the support of the 3D Fourier transform of H , namely, the optical transfer function (OTF). Throughout this paper, we define the transverse (in the plane normal to $\hat{\mathbf{z}}$) and axial resolutions of the microscope to be inversely proportional to the span of the OTF along these directions.

A. Point Detection: Transmission Holography and Full-Field Coherent OCT

Let us first consider a configuration with a point detector and point source for which the point spread function reads $H_{\text{point}}(\mathbf{r}) \propto k_0^2 G(\mathbf{r}, \mathbf{i}) G(\mathbf{o}, \mathbf{r})$, where $(\mathbf{i}, \mathbf{o}, \mathbf{r})$ indicate points in the illumination, observation, and sample domains, respectively. This configuration corresponds to any full-field coherent microscope in which the sample is illuminated by a coherent

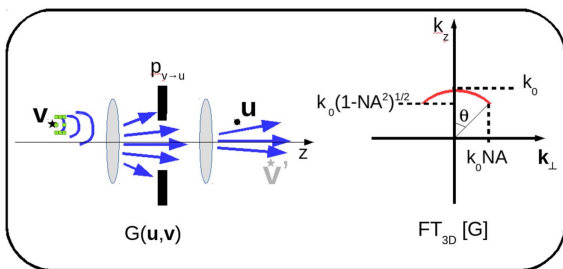


Fig. 3. Illustration of $G(\mathbf{v}, \mathbf{u})$ in a standard microscope mounted in a $4f$ configuration. The 3D Fourier transform of G , $\text{FT}_{3D}[G]$, is rotationally invariant about the k_z axis.

plane wave $G(\mathbf{r}, \mathbf{i}) = \exp(i\mathbf{k}_i \cdot \mathbf{r})$, stemming from a point source in the far field, and the interference term is detected on camera pixels. Examples are full-field coherent OCT [3] and transmission-mode holography [7].

The support of the OTF in this simple case is the cap of sphere corresponding to the Fourier transform of $G(\mathbf{o}, \mathbf{r})$ translated by \mathbf{k}_i —see Fig. 4(a).

In the reflection configuration where $\mathbf{k}_i = -k_0 \hat{\mathbf{z}}_{r \rightarrow o}$, the OTF is a cap of sphere passing through the point $2k_0 \hat{\mathbf{z}}_{r \rightarrow o}$. In the transmission configuration, where $\mathbf{k}_i = k_0 \hat{\mathbf{z}}_{r \rightarrow o}$, the OTF is a cap of sphere passing through the origin. In both cases, the transverse extension of the OTF is $2k_0 \text{NA}$, yielding a transverse resolution about $\lambda/(2\text{NA})$, and the axial extension is $(k_0 - k_{\text{min}})$, where $k_{\text{min}} = k_0 \cos \theta = k_0 \sqrt{1 - \text{NA}^2}$. Despite the surface shape of the OTF, which impedes 3D imaging in general, one can estimate an approximate axial resolution of about $2\lambda/\text{NA}^2$ for small NA and samples comprising point objects. However, neither case provides optical sectioning since the image of a thin transverse object becomes infinitely extended along the z direction.

To obtain axial sectioning the use of white or pulsed light is mandatory. Denoting as $[k^+, k^-]$ the spectral range of the source (in wavenumber units) and recalling the equivalence of pulsed and continuous illumination of equal spectral range, the point spread function becomes proportional to $\int_{k^-}^{k^+} H_{\text{point}}(\mathbf{r}, k_0) dk_0$, where the dependency of H_{point} on k_0 is now made explicit. The extension of the OTF along k_z in the reflection configuration is now $2(k^+ - k^-)$ [see Fig. 4(b) (blue)], which provides both optical sectioning and an axial resolution of about $\pi/(k^+ - k^-)$. However, this benefit that comes from a broad spectral range largely disappears in the transmission configuration, as shown in Fig. 4(b) (red). In particular, the OTF extension at $k_\perp = 0$ remains null, meaning that optical sectioning is

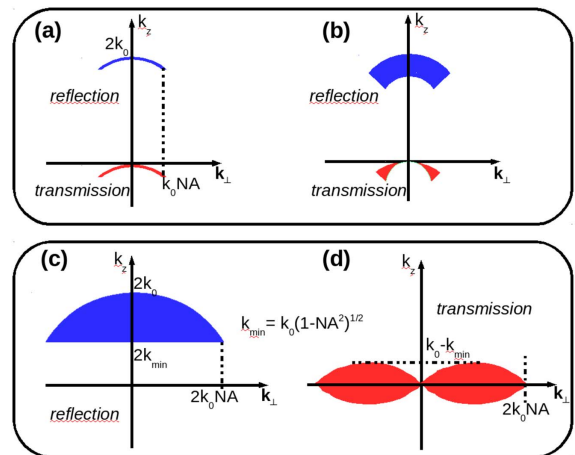


Fig. 4. Support of the OTF of various microscopes. (a) Monochromatic transmission and reflection holography using plane-wave illumination. (b) Same as (a) but with pulsed or white light (corresponding to full-field coherent OCT in reflection). (c) Monochromatic reflection holography using focused or incoherent illumination (scanning OCT, full-field incoherent OCT, confocal reflectance microscopy). (d) Same as (c) but in transmission (corresponding to classical bright-field transmission microscopy). All the OTFs are rotationally invariant about the k_z axis.

not recovered. As a result, white-light illumination in transmission digital holography does not significantly outperform monochromatic illumination.

B. Full Reference-Field Detection

We now consider configurations where the detector is large enough to collect the full reference field $G(\mathbf{o}, \mathbf{i})$ (i.e., the field existing in the absence of the sample) propagating toward the positive (in the transmission configuration) or negative (in the reflection configuration) z . In this case, the point spread functions are given by (H_R, H_T) in Eqs. (10) and (11).

In practice, these configurations can be achieved by placing the detector in the observation pupil (i.e., the observation Fourier plane) and ensuring that its size fully encompasses all the pupils within the microscope. As a result, the point spread function depends only on the illumination pupil $p_{i \rightarrow r}$ with numerical aperture NA. In the (equivalent by reciprocity) full-field configuration with extended incoherent sources, the full reference-field detection imposes that the illumination pupil is similar or larger than the collection pupil. In the usual terminology, this corresponds to fully incoherent illumination [1].

1. Reflection Configuration: Scanning and Full-Field Incoherent OCT

The reflection configuration with a point source and large detector corresponds to conventional time-domain scanning OCT, which scans a focused beam inside the sample (corresponding to a source located in a plane conjugate to the focal plane) and collects all the reflected light [8]. Because of the reciprocity theorem, it also corresponds to full-field incoherent OCT where the illumination is provided by a surface of incoherent sources and the reflected field is detected by a camera, as described in [9]. In this case, the roles of \mathbf{i} and \mathbf{o} are reversed. For equal NA, scanning OCT [8], full-field incoherent OCT [9], and, H_R being similar to H_{confocal} , interferometric confocal microscopy (such as an optical coherence microscope [10]), theoretically provide the same resolution.

The reflection point spread function is given by $H_R(\mathbf{r}) = \frac{k_0}{2z} G^2(\mathbf{r}, \mathbf{i})$ [Eq. (10)]. Hence, the support of the OTF is given by the self-convolution of the cap of sphere of radius k_0 corresponding to $G(\mathbf{r}, \mathbf{i})$, which results in a filled-in section of a ball of radius $2k_0$, as depicted in Fig. 4(c). The extension of the OTF in the transverse plane is $4k_0\text{NA}$, which yields a theoretically achievable resolution about $0.25\lambda/\text{NA}$ [11], while that in the axial direction is about $2k_0(1 - \sqrt{1 - \text{NA}^2})$, which yields a resolution about $\lambda/(4\text{NA}^2)$.

The extension of the OTF along the z -axis being non-null for $k_{\perp} = 0$, these kinds of microscopes exhibit optical sectioning even with monochromatic illumination. Indeed, as long as $k^+ - k^- < 2k^+(1 - \sqrt{1 - \text{NA}^2})$ the angular diversity of the illumination at the highest frequency is sufficient to provide an axial resolution equivalent to that of the polychromatic microscope. Thus, using white light or pulsed laser will not improve significantly the optical sectioning if $\text{NA} > 0.85$.

2. Transmission Configuration: Bright-Field Transmission Microscopy

A same analysis can be carried out for the transmission configuration. Scanning and full-field incoherent interferometric

microscopes in transmission mode are less prevalent than their reflection counterparts, though some implementations using an independent reference arm exist [12]. On the other hand, without the complex interference measurement, the full-field incoherent configuration in transmission is very widespread as it corresponds to the conventional bright-field microscope [1].

The transmission point spread function is given by $H_T(\mathbf{r}) = -\frac{k_0}{2z} |G|^2(\mathbf{r}, \mathbf{i})$ [Eq. (11)]. Hence, the support of the OTF is given by the self-correlation of the cap of sphere corresponding to $G(\mathbf{r}, \mathbf{i})$. The result is a torus-shaped volume of diameter $4k_0\text{NA}$, as depicted in Fig. 4(d), yielding a transverse resolution similar to the reflection mode of about $\lambda/(4\text{NA})$. On the other hand, because the extension of the OTF along the z -axis is null for $k_{\perp} = 0$, optical sectioning remains impossible regardless of whether the illumination is white-light or pulsed.

Manifestly, there is a major difference between the reflection and the transmission configurations. Comparing the OTFs in Figs. 4(c) and 4(d), one can easily point out their associated advantages and drawbacks. The reflection OTF allows optical sectioning but filters out the low axial sample frequencies. The transmission OTF does not allow optical sectioning but is adapted to smooth, slowly varying samples.

We have assumed throughout this section that interferometric measurements enabled a retrieval of the complex interference term D , Eq. (4). This complex term, in turn, provides sample absorption ($\delta\epsilon$ is imaginary) and phase ($\delta\epsilon$ is real) maps, though usually with different point spread functions since H is complex. In a standard bright-field microscope, only the real part $\Re(D)$ of the interference term is detected. Accordingly, since the point spread function of the microscope given by Eq. (11) is purely imaginary, only the sample absorption map can be retrieved from the data (appearing as a shadow in a bright background) [1].

C. Partial Reference-Field Detection: Phase Microscopy

We now turn to the more complex configuration where, in the absence of the sample, the detector does not collect all the reference field. This occurs when the observation pupil, where the detector resides, does not fully encompass all other pupils within the microscope. In the (equivalent by reciprocity) full-field configuration with extended incoherent sources, it corresponds in particular to illumination pupils that are smaller than the collection pupil, namely, to partially coherent illumination [1]. In this case, the microscope point spread function is given by Eq. (5). Examples of microscopes based on partial reference-field detection are Zernike phase contrast [13] (where the illumination pupil is annular and included within the observation pupil, and we invoke the reciprocity theorem to exchange the roles of \mathbf{o} and \mathbf{i}) or oblique-field microscope (where the illumination and detection pupils are laterally shifted relative to one another [14,15]). All these microscopes take advantage of the fact that the point spread function given by Eq. (5) is complex, enabling them to perform phase imaging.

D. No Reference-Field Detection: Dark-Field and Reflectance Confocal Microscopy

Finally, we consider the particular case where, in the absence of the sample, the detector does not collect anything; that is,

$G(\mathbf{o}, \mathbf{i}) = 0$ whatever $\mathbf{o} \in \Gamma$. This occurs when the illumination and observation pupils do not intersect, as in dark-field or reflectance confocal microscopy. In these cases, the detector is sensitive to $|\delta E(\mathbf{o}, \mathbf{i})|^2$, as obtained from Eq. (3), which reads

$$|\delta E(\mathbf{o}, \mathbf{i})|^2 = k_0^4 \int_{W \times W} F(\mathbf{o}, \mathbf{r}_1, \mathbf{r}_2) \delta \epsilon(\mathbf{r}_1) \delta \epsilon^*(\mathbf{r}_2) F(\mathbf{i}, \mathbf{r}_1, \mathbf{r}_2) d\mathbf{r}_1^3 d\mathbf{r}_2^3, \quad (13)$$

where $F(\mathbf{a}, \mathbf{r}_1, \mathbf{r}_2) = G(\mathbf{a}, \mathbf{r}_1) G^*(\mathbf{a}, \mathbf{r}_2)$. The measurement is thus non-linearly linked to $\delta \epsilon$, meaning that, except for slowly varying samples that are homogeneous over the typical size of the focus spot $G(\mathbf{r}, \mathbf{i})$, there is no simple link between the image and the object.

APPENDIX A: SCALAR FIELDS

In this appendix, we provide derivations of the volume integral equation satisfied by the field in the presence of the sample, the reciprocity theorem, and the time-reversal identity.

Let ϵ_m be the relative permittivity distribution in the microscope without the sample and $\epsilon_m + \delta \epsilon$ be the relative permittivity in the presence of the sample. We call $E(\mathbf{r}, \mathbf{i})$ the field created in the microscope in the presence of the sample by a point source placed at \mathbf{i} . E is the solution to the equation

$$\nabla^2 E(\mathbf{r}, \mathbf{i}) + k_0^2 \epsilon_m(\mathbf{r}) E(\mathbf{r}, \mathbf{i}) = -\delta(\mathbf{r} - \mathbf{i}) - k_0^2 \delta \epsilon(\mathbf{r}) E(\mathbf{r}, \mathbf{i}), \quad (A1)$$

which satisfies an outgoing wave boundary condition. We now introduce the Green function of the microscope, $G(\mathbf{r}, \mathbf{r}')$, which is the solution of

$$\nabla_r^2 G(\mathbf{r}, \mathbf{r}') + k_0^2 \epsilon_m(\mathbf{r}) G(\mathbf{r}, \mathbf{r}') = -\delta(\mathbf{r} - \mathbf{r}'), \quad (A2)$$

which also satisfies an outgoing wave boundary condition. We readily obtain the domain integral equation for E , valid for all \mathbf{o} :

$$E(\mathbf{o}, \mathbf{i}) = G(\mathbf{o}, \mathbf{i}) + k_0^2 \int_W G(\mathbf{o}, \mathbf{r}) \delta \epsilon(\mathbf{r}) E(\mathbf{r}, \mathbf{i}) d^3 \mathbf{r}. \quad (A3)$$

The reciprocity theorem is demonstrated from the scalar Green identity, which states that for any $U(\mathbf{r}')$ and $V(\mathbf{r}')$ fields,

$$\int_{\text{Vol}} U \nabla^2 V - V \nabla^2 U d^3 \mathbf{r}' = \int_S (U \nabla V - V \nabla U) \cdot \mathbf{n} d^2 \mathbf{r}', \quad (A4)$$

where Vol is a volume delimited by the surface S and $\mathbf{n}(\mathbf{r}')$ is the normal to S pointing outwards. We take S to be a far-field sphere enclosing the microscope elements, the sample, the source, and the detectors. In this case, $\mathbf{n} = \hat{\mathbf{r}}'$ where $\hat{\mathbf{r}}' = \mathbf{r}'/r'$. We also take $U(\mathbf{r}') = E(\mathbf{r}', \mathbf{i})$, $V(\mathbf{r}') = E(\mathbf{r}', \mathbf{o})$. Bearing in mind that in the far-field $\nabla E(\mathbf{r}') = ik_0 E(\mathbf{r}') \hat{\mathbf{r}}'$, one easily shows that the right-hand term of Eq. (A4) is equal to 0. Using Eq. (A1) on the left-hand side of Eq. (A4), one obtains the reciprocity relation:

$$E(\mathbf{o}, \mathbf{i}) = E(\mathbf{i}, \mathbf{o}). \quad (A5)$$

The time-reversal identity is obtained in a similar manner by taking $U(\mathbf{r}') = G^*(\mathbf{r}', \mathbf{i})$ and $V(\mathbf{r}') = G(\mathbf{r}', \mathbf{r})$ in Eq. (A4) and S a sphere large enough to be in the far field of both \mathbf{r} (which belongs to the sample domain) and \mathbf{i} (which belongs to the illumination domain). In practice, S represents the detector surface over which the field intensity is integrated.

Now, in the far field $\nabla G^*(\mathbf{r}', \mathbf{i}) = -ik_0 G^*(\mathbf{r}', \mathbf{i}) \hat{\mathbf{r}}'$ while $\nabla G(\mathbf{r}', \mathbf{r}) = ik_0 G(\mathbf{r}', \mathbf{r}) \hat{\mathbf{r}}'$ so that the right-hand term of Eq. (A4) no longer cancels, but instead becomes $2ik_0 \int_S G(\mathbf{r}', \mathbf{r}) G^*(\mathbf{r}', \mathbf{i}) d^3 \mathbf{r}'$. Assuming that ϵ_m is real so that both G and G^* satisfy Eq. (A2), the left-hand side of Eq. (A4) yields $[G(\mathbf{r}, \mathbf{i}) - G^*(\mathbf{r}, \mathbf{i})]$. One finally obtains

$$\int_S G^*(\mathbf{r}', \mathbf{i}) G(\mathbf{r}', \mathbf{r}) d^2 \mathbf{r}' = \frac{1}{2ik_0} [G(\mathbf{r}, \mathbf{i}) - G^*(\mathbf{r}, \mathbf{i})]. \quad (A6)$$

APPENDIX B: VECTOR FIELDS

In this appendix, we describe the extension of our analysis to the full vectorial case. For more generality, the microscope and sample can contain anisotropic elements. We introduce $\bar{\epsilon}_m$ the relative permittivity tensor of the microscope without the sample, and $\bar{\epsilon}_m + \delta \bar{\epsilon}$ the relative permittivity in the presence of the sample. Hereafter, we assume that the permittivity tensor of the microscope is reciprocal, meaning that ${}^t \bar{\epsilon}_m = \bar{\epsilon}_m$.

We call $\mathbf{E}(\mathbf{r}, \mathbf{i})$ the vectorial field created at \mathbf{r} in the microscope *in the presence of the sample* by the vectorial point source \mathbf{p}_i placed at \mathbf{i} . The field \mathbf{E} is the solution of the equation

$$\nabla \times \nabla \times \mathbf{E}(\mathbf{r}, \mathbf{i}) - k_0^2 \bar{\epsilon}_m(\mathbf{r}) \mathbf{E}(\mathbf{r}, \mathbf{i}) = \mathbf{p}_i \delta(\mathbf{r} - \mathbf{i}) + k_0^2 \delta \bar{\epsilon}(\mathbf{r}) \mathbf{E}(\mathbf{r}, \mathbf{i}), \quad (B1)$$

which satisfies an outgoing wave boundary condition.

We now introduce the Green tensor of the microscope, $\bar{\mathbf{G}}(\mathbf{r}, \mathbf{r}')$, which is the solution of

$$\nabla \times \nabla \times \bar{\mathbf{G}}(\mathbf{r}, \mathbf{r}') - k_0^2 \bar{\epsilon}_m(\mathbf{r}) \bar{\mathbf{G}}(\mathbf{r}, \mathbf{r}') = \delta(\mathbf{r} - \mathbf{r}') \bar{\mathbf{I}}, \quad (B2)$$

which satisfies an outgoing wave boundary condition. We readily obtain the domain integral equation for \mathbf{E} , valid for all \mathbf{o} ,

$$\mathbf{E}(\mathbf{o}, \mathbf{i}) = \bar{\mathbf{G}}(\mathbf{o}, \mathbf{i}) \mathbf{p}_i + k_0^2 \int_W \bar{\mathbf{G}}(\mathbf{o}, \mathbf{r}) \delta \bar{\epsilon}(\mathbf{r}) \mathbf{E}(\mathbf{r}, \mathbf{i}) d^3 \mathbf{r}, \quad (B3)$$

from which we obtain the expression of the scattered field under the Born approximation,

$$\delta \mathbf{E}(\mathbf{o}, \mathbf{i}) \approx k_0^2 \int_W \bar{\mathbf{G}}(\mathbf{o}, \mathbf{r}) \delta \bar{\epsilon}(\mathbf{r}) \bar{\mathbf{G}}(\mathbf{r}, \mathbf{i}) \mathbf{p}_i d^3 \mathbf{r}. \quad (B4)$$

The reciprocity theorem is demonstrated from the vectorial Green identity, which states that for any vectorial field $\mathbf{U}(\mathbf{r}')$ and $\mathbf{V}(\mathbf{r}')$,

$$\int_{\text{Vol}} \mathbf{U} \cdot \nabla \times \nabla \times \mathbf{V} - \mathbf{V} \cdot \nabla \times \nabla \times \mathbf{U} d^3 \mathbf{r}', \quad (B5)$$

$$= \int_S (\mathbf{V} \times \nabla \times \mathbf{U} - \mathbf{U} \times \nabla \times \mathbf{V}) \cdot \mathbf{n} d^2 \mathbf{r}', \quad (B6)$$

where Vol is a volume delimited by the surface S and \mathbf{n} is the normal to S pointing outwards.

Following the same procedure as in the scalar case, we consider S to be a far-field sphere encompassing the microscope, the sample, the sources, and the detectors. The reciprocity theorem is obtained by taking $\mathbf{U}(\mathbf{r}') = \mathbf{E}(\mathbf{r}', \mathbf{i})$ and $\mathbf{V}(\mathbf{r}') = \mathbf{E}(\mathbf{r}', \mathbf{o})$. Bearing in mind that, in the far field, $\nabla \times \mathbf{E}(\mathbf{r}') = ik_0 \hat{\mathbf{r}}' \times \mathbf{E}(\mathbf{r}')$ and $\mathbf{E}(\mathbf{r}') \cdot \mathbf{r}' = 0$, one easily shows that the right-hand term of Eq. (B6) is equal to 0. Inserting Eq. (B1) in the left-hand side of Eq. (B6) and using the property

$$\overline{\mathbf{M}}\mathbf{V} \cdot \mathbf{U} = {}^t\overline{\mathbf{M}}\mathbf{U} \cdot \mathbf{V} \quad (\text{B7})$$

with ${}^t\overline{\epsilon}_m = \overline{\epsilon}_m$, the left-hand side of Eq. (B6) is then $\mathbf{E}(\mathbf{o}, \mathbf{i}) \cdot \mathbf{p}_o - \mathbf{E}(\mathbf{i}, \mathbf{o}) \cdot \mathbf{p}_i$.

Equating the left- and right-hand sides of the Green identity, one obtains the vectorial reciprocity theorem valid for any reciprocal inhomogeneous medium [16]:

$$\mathbf{E}(\mathbf{o}, \mathbf{i}) \cdot \mathbf{p}_o = \mathbf{E}(\mathbf{i}, \mathbf{o}) \cdot \mathbf{p}_i. \quad (\text{B8})$$

The time-reversal identity is obtained in a similar manner by taking $\mathbf{U}(\mathbf{r}') = \overline{\mathbf{G}}^*(\mathbf{r}', \mathbf{i})\mathbf{p}_i^*$ and $\mathbf{V}(\mathbf{r}') = \overline{\mathbf{G}}(\mathbf{r}', \mathbf{r})\mathbf{p}_r$ in Eq. (B6). Now, in the far field $\nabla \times \overline{\mathbf{G}}^*(\mathbf{r}', \mathbf{i})\mathbf{p}_i^* = -ik_0\hat{\mathbf{r}}' \times \overline{\mathbf{G}}^*(\mathbf{r}', \mathbf{i})\mathbf{p}_i^*$ while $\nabla \times \overline{\mathbf{G}}(\mathbf{r}', \mathbf{r})\mathbf{p}_r = ik_0\hat{\mathbf{r}}' \times \overline{\mathbf{G}}(\mathbf{r}', \mathbf{r})\mathbf{p}_r$, so that the right-hand term of Eq. (B6) no longer cancels but instead becomes $-2ik_0 \int_S \overline{\mathbf{G}}^*(\mathbf{r}', \mathbf{i})\mathbf{p}_i^* \cdot \overline{\mathbf{G}}(\mathbf{r}', \mathbf{r})\mathbf{p}_r d^3r'$. Using Eq. (B7), the right-hand term can also be written as $-2ik_0\mathbf{p}_r \cdot \int_S \overline{\mathbf{G}}(\mathbf{r}, \mathbf{r}')\overline{\mathbf{G}}^*(\mathbf{r}', \mathbf{i})\mathbf{p}_i^* d^2r'$.

Assuming that $\overline{\epsilon}_m$ is real so that $\overline{\mathbf{G}}^*(\mathbf{r}', \mathbf{i})$ satisfies also Eq. (B2), the left-hand side of Eq. (B6) can be written as $\overline{\mathbf{G}}(\mathbf{i}, \mathbf{r})\mathbf{p}_r \cdot \mathbf{p}_i^* - \overline{\mathbf{G}}^*(\mathbf{r}, \mathbf{i})\mathbf{p}_i^* \cdot \mathbf{p}_r$, which is equal to $[\overline{\mathbf{G}}(\mathbf{r}, \mathbf{i})\mathbf{p}_i^* - \overline{\mathbf{G}}^*(\mathbf{r}, \mathbf{i})\mathbf{p}_i^*] \cdot \mathbf{p}_r$.

Equating the two sides of the vectorial Green identity yields the vectorial time-reversal identity [5]:

$$\int_S \overline{\mathbf{G}}(\mathbf{r}, \mathbf{r}')\overline{\mathbf{G}}^*(\mathbf{r}', \mathbf{i})\mathbf{p}_i^* d^2r' = \frac{1}{2ik_0}[\overline{\mathbf{G}}(\mathbf{r}, \mathbf{i})\mathbf{p}_i^* - \overline{\mathbf{G}}^*(\mathbf{r}, \mathbf{i})\mathbf{p}_i^*]. \quad (\text{B9})$$

Following the same demonstration as in the scalar case, Eq. (B9) can be readily used to provide the point spread function of the vectorial microscope when the detector is large enough to collect all the light on either side of the microscope (reflection or transmission).

We first derive the expression of the complex interference term D between the scattered field, Eq. (B4), and the reference field integrated over the detector,

$$D = \int_{\Gamma} \overline{\mathbf{G}}^*(\mathbf{o}, \mathbf{i})\mathbf{p}_i^* \cdot k_0^2 \int_W \overline{\mathbf{G}}(\mathbf{o}, \mathbf{r})\overline{\delta\epsilon}(\mathbf{r})\overline{\mathbf{G}}(\mathbf{r}, \mathbf{i})\mathbf{p}_i d^3rd^2o, \quad (\text{B10})$$

which can be rewritten, using the reciprocity theorem,

$$D = k_0^2 \int_W \overline{\delta\epsilon}(\mathbf{r})\overline{\mathbf{G}}(\mathbf{r}, \mathbf{i})\mathbf{p}_i \cdot \int_{\Gamma} \overline{\mathbf{G}}(\mathbf{r}, \mathbf{o})\overline{\mathbf{G}}^*(\mathbf{o}, \mathbf{i})\mathbf{p}_i^* d^3rd^2o. \quad (\text{B11})$$

Then, using Eq. (B9) and the propagation properties of the vectorial fields illustrated in Fig. 2, one obtains in transmission,

$$D_T = -\frac{k_0}{2i} \int_W \overline{\delta\epsilon}(\mathbf{r})\overline{\mathbf{G}}(\mathbf{r}, \mathbf{i})\mathbf{p}_i \cdot \overline{\mathbf{G}}^*(\mathbf{r}, \mathbf{i})\mathbf{p}_i^* d^3r, \quad (\text{B12})$$

and in reflection,

$$D_R = \frac{k_0}{2i} \int_W \overline{\delta\epsilon}(\mathbf{r})\overline{\mathbf{G}}(\mathbf{r}, \mathbf{i})\mathbf{p}_i \cdot \overline{\mathbf{G}}(\mathbf{r}, \mathbf{i})\mathbf{p}_i^* d^3r. \quad (\text{B13})$$

In the simplified case where the sample can be described by a scalar permittivity contrast $\delta\epsilon$, one can define a point spread function in transmission,

$$H_T(\mathbf{r}) = -\frac{k_0}{2i} |\overline{\mathbf{G}}(\mathbf{r}, \mathbf{i})\mathbf{p}_i|^2, \quad (\text{B14})$$

and in reflection,

$$H_R(\mathbf{r}) = \frac{k_0}{2i} \overline{\mathbf{G}}(\mathbf{r}, \mathbf{i})\mathbf{p}_i^* \cdot \overline{\mathbf{G}}(\mathbf{r}, \mathbf{i})\mathbf{p}_i. \quad (\text{B15})$$

When the detector is a point placed at \mathbf{o} , the recorded interference term D reads

$$D_{\text{point}} = k_0^2 \overline{\mathbf{G}}^*(\mathbf{o}, \mathbf{i})\mathbf{p}_i^* \cdot \int_W \overline{\mathbf{G}}(\mathbf{o}, \mathbf{r})\overline{\delta\epsilon}(\mathbf{r})\overline{\mathbf{G}}(\mathbf{r}, \mathbf{i})\mathbf{p}_i d^3r. \quad (\text{B16})$$

For a microscope in a confocal configuration and a sample described by a scalar permittivity contrast, Eq. (B16) leads to the confocal point spread function, which is, as expected, similar to H_R :

$$H_{\text{confocal}} \propto k_0^2 \overline{\mathbf{G}}(\mathbf{r}, \mathbf{i})\mathbf{p}_i^* \cdot \overline{\mathbf{G}}(\mathbf{r}, \mathbf{i})\mathbf{p}_i. \quad (\text{B17})$$

To our knowledge, these are the first derivations of fully vectorial point spread functions that make allowances for anisotropic samples.

Funding. ITMO Cancer (20014-2019); National Institutes of Health (NIH) (R01CA182939).

REFERENCES AND NOTES

1. N. Streibl, "Three-dimensional imaging by a microscope," *J. Opt. Soc. Am. A* **2**, 121–127 (1985).
2. C. J. R. Sheppard and T. Wilson, "On the equivalence of scanning and conventional microscopes," *Optik* **73**, 39–43 (1986).
3. D. L. Marks, T. S. Ralston, S. A. Boppert, and P. Scott Carney, "Inverse scattering for frequency-scanned full-field optical coherence tomography," *J. Opt. Soc. Am. A* **24**, 1034–1041 (2007).
4. Moving the sample yields a correlation while moving the source [in a translationally invariant microscope where $G(r, i) = G(r - i)$] yields a convolution. In most cases, the source is moved in the transverse plane while the sample is moved along the axial direction. For a more in-depth discussion of this difficulty, see D. S. Goodman, "Stationary optical projectors," Ph.D. dissertation (University of Arizona, 1979), <http://hdl.handle.net/10150/298640>, Chap. 10.
5. R. Carminati, R. Pierrat, J. de Rosny, and M. Fink, "Theory of the time reversal cavity for electromagnetic fields," *Opt. Lett.* **32**, 3107–3109 (2007).
6. C. J. R. Sheppard, S. S. Kou, and J. Lin, "The Green-function transform and wave propagation," *Front. Phys.* **2**, 1–10 (2014).
7. D. Gabor, "A new microscope principle," *Nature* **161**, 777–778 (1948).
8. D. Huang, E. A. Swanson, C. P. Lin, J. S. Schuman, W. G. Stinson, W. Chang, M. R. Hee, T. Flotte, K. Gregory, C. A. Puliafito, and J. G. Fujimoto, "Optical coherence tomography," *Science* **254**, 1178–1181 (1991).
9. E. Beaufort, A. C. Bocarra, M. Lebec, L. Blanchot, and H. Saint-Jalmes, "Full-field optical coherence microscopy," *Opt. Lett.* **23**, 244–246 (1998).
10. J. A. Izatt, M. R. Hee, G. M. Owen, E. A. Swanson, and J. G. Fujimoto, "Optical coherence microscopy in scattering media," *Opt. Lett.* **19**, 590–592 (1994).
11. O. Haeberlé, K. Belkebir, H. Giovannini, and A. Sentenac, "An introduction to diffractive tomographic microscopy," *J. Mod. Opt.* **57**, 686–699 (2010).
12. J. Dyson, "An interferometer microscope," *Proc. R. Soc. A* **204**, 170–187 (1950).
13. F. Zernike, "How I discovered phase contrast," *Science* **121**, 345–349 (1955).
14. S. B. Mehta and C. J. R. Sheppard, "Quantitative phase-gradient imaging at high resolution with asymmetric illumination-based differential phase contrast," *Opt. Lett.* **34**, 1924–1926 (2009).
15. R. Barankov, J.-C. Baritaux, and J. Mertz, "High-resolution 3D phase imaging using a partitioned detection aperture: a wave-optic analysis," *J. Opt. Soc. Am. A* **32**, 2123–2135 (2015).
16. L. Landau, E. Lifshitz, and L. Pitaevskii, *Electrodynamics of Continuous Media* (Pergamon, 1984).